

The Overlapping Control Volume Finite Element Method for Multi-Fluids Porous Media Flow Modelling. Part II: Simulation Results

D. Pavlidis^{a,*}, J.L.M.A. Gomes^b, J.R. Percival^a, P. Mostaghimi^a, P. Salinas^a, Z. Xie^a, C.C. Pain^a, M. D. Jackson^a, A.H. ELSheikh^c, M. Blunt^a, A. Muggaridge^a

^a*Applied Modelling and Computation Group, Department of Earth Science and Engineering, Imperial College London, UK*

^b*Environmental & Industrial Fluids Mechanics Group, School of Engineering, University of Aberdeen, UK*

^c*Institute of Computational Engineering and Science, University of Texas at Austin, USA*

Abstract

This is the second part of a two part paper on the overlapping finite element method applied to porous media multiphase flows. In the first part we dealt with the formulation. In this second part we demonstrate the results from the overlapping control volume finite element method (OCV-FEM). We first apply the model to situations with known analytical results and show the order of convergence of the various element types, discontinuous in velocity and continuous in pressure elements P_nDG-P_n+1 as well as fully discontinuous elements P_nDG-P_nDG. We then proceed to model a number of test cases to show how the methods compare for a range of test cases.

Keywords: Multiphase Darcy Equations, Discontinuous Galerkin method, Overlapping mixing formulation

Contents

1	Introduction	2
----------	---------------------	----------

*Corresponding author.

Email address: dimitrios.pavlidis04@imperial.ac.uk ()

2	The Buckley-Leverett test case	2
2.1	Convergence analysis	3
2.2	Numerical experiments	4
3	A 4-region modified Buckley-Levrett test case	4
4	An embedded-region modified Buckley-Leverett test case	6
5	A wedge-shaped modified Buckley-Leverett test case	6
6	Conclusions	7
	Acknowledgements	7

1. Introduction

A few paragraphs introducing generic applications for the model on reservoir simulations, CCS, waste repositories, transport of pollutants etc. Also a paragraph highlighting the importance of an efficient test-matrix for the new CMFD for porous media.

This is the second of a series of papers exploiting novel computational methods for multi-fluids flow in porous media. The new overlapping control volume finite element method was introduced in the first part of this series followed by an advection test-case validation (Gomes et al., 2013). The formulation lies in two-folds development, it uses a dual consistent pressure-velocity representation in CV and FEM spaces (through a mixing formulation) and a recently developed $P_n DGP_{n+1}$ family of FE types. Additionally a novel family of fully discontinuous element types – the $P_n DGP_n DG$, was introduced to represent discontinuity across neighbor elements leading to a highly heterogeneous porous media domain, typical of some geological formations.

2. The Buckley-Leverett test case

The one-dimensional incompressible Buckley-Leverett equations with gas injection along a fully saturated ($S_f = 1$) bore hole of uniform porosity ($\phi = 0.5$) are modelled using Porosity. The gas is injected at a velocity of $u_g = 1$ and a saturation of $S_g = 1$. On the outflow boundary the pressure level is set to zero. The length of the bore hole is 4 non-dimensional units.

All boundary conditions are applied weakly. The Corey model defined as: $k_g = S_g^{-2}$ is used to calculate the relative permeability.

All simulations use the overlapping mixed finite element method and a number of element pairs (for velocity and pressure) are evaluated. Saturation is collocated at the pressure nodes. Although saturation is calculated using a control volume formulation a FEM interpolation is used to form the high order fluxes and this is also used here for most of the saturation plots. Fig. 1 shows the CV saturation of gas (with horizontal and vertical lines) and the quadratic finite element interpolation (FEM interpolation). The solution converges with increased resolution. Note that the right corners of the control volumes agree best with the analytical solution. This is because up-winding of the velocities is used (or equivalently the relative permeabilities) and it is at these points that the equations reach the balance necessary to match closely the analytic solution.

Despite the one-dimensional nature of the problem, it is reproduced in two and three dimensions using structured and unstructured meshes to evaluate the multi-dimensional capabilities of the model. In two- and three-dimensional simulations, free-slip boundary conditions are applied on the sides of the domain for the two velocity fields.

2.1. Convergence analysis

A convergence analysis is undertaken for one and two dimensions. A number of meshes and element pairs are assessed with respect to the gas phase saturation field.

All one-dimensional meshes have equi-sized elements. Two-dimensional meshes are structured and one-element wide. Their elements are also equi-sized and have unity aspect ratio. Thus the width of the two-dimensional domains is inversely proportional to the number of elements. The time step size is linearly varied between $1.25 \cdot 10^{-4}$ and $3.125 \cdot 10^{-3}$ for the one-dimensional simulations, while it is 10^{-4} for all two-dimensional simulations.

Saturation profiles for the gas phase at time $t = 0.5$ are shown in Fig. 6. One dimension P0DG-P1 profiles for meshes having between 5 and 100 elements are shown on the top left. One dimension P1DG-P2 and P2DG-P3 profiles for meshes having between 5 and 500 elements are shown on the top right and bottom left, respectively. Finally, two dimension P1DG-P2 profiles for meshes having between 5 and 100 elements are shown on the bottom right. The geometry symmetry line is used to extract data for the two-dimensional simulation.

Results are in good agreement with the analytic solution even for the coarse meshes and in all four cases the results converge to the analytical solution with increasing resolution.

Note that for the coarse meshes (5 and 20 elements) high-order elements perform better and are able to capture the front more accurately. Consequently, P1DG-P2 performs better than P0DG-P1 and P2DG-P3 performs better than P1DG-P2. As far as the two-dimensional simulations are concerned, the coarse mesh simulation performs slightly worse than its one-dimensional counterpart but for higher resolutions results are identical.

These conclusions become clearer in Fig. 7, where convergence rates are shown. The L1 error defined as $N^{-1}\sum_{i=1}^N|y_i - E_i|$ is shown on the left, while the L2 error defined as $N^{-1}(\sum_{i=1}^N(y_i - E_i)^2)^{0.5}$ is shown on the right (y represents modelled gas phase saturations and E represents analytic gas phase saturations). In addition to the simulations discussed so far, convergence rates for another set simulations that use full upwinding is also shown in Fig. 7. *** ADD DISCUSSION HERE ***

2.2. Numerical experiments

Following the convergence analysis a number of numerical experiments are performed to evaluate the robustness of the method in fully unstructured meshes.

Gas phase saturation surface maps for a two- and a three-dimensional simulation at time $t = 0.5$ are shown in Fig. 5. The mesh and surface mesh for the two- and three-dimensional simulations, respectively, are also shown in Fig. 5. These simulations use unstructured meshes and the P1DGP2 element pair.

Saturation profiles for the gas phase at time $t = 0.5$ are shown in Fig. 6. Results are not spatially averaged and the geometry symmetry line is used to extract data for all simulations. The structured coarse mesh uses 1×19 layers in the lateral and flow directions, respectively. The structured medium mesh uses 3×40 layers.

3. A 4-region modified Buckley-Levrett test case

A four-region modified Buckley-Levrett test case is used to demonstrate the capabilities of the suggested method. In this test case gas is injected in a fully saturated ($S_f = 1$) two-dimensional square domain of side length one and uniform porosity ($\phi = 0.5$). However, unlike the original Buckley-Levrett

test case, the permeability of the domain is not uniform and four ‘regions’ exist. A schematic of the geometry along with the four regions and boundary conditions is shown in Fig. 8. The four regions are square and equi-sized. The permeability in regions R1 and R4 is 4 times bigger than that of regions R2 and R3.

The gas is injected at a velocity of $u_g = 1$ and a saturation of $S_g = 1$. On the outflow boundary the pressure level is set to zero. Free-slip boundary conditions are applied on the sides of the domain for the two velocity fields. All boundary conditions are applied weakly. The Corey model defined as: $k_g = S_g^{-2}$ is used to calculate the relative permeability.

All simulations use the overlapping mixed finite element method and the P1DG-P2 element pair. The time step sizes are 10^{-3} and $5 \cdot 10^{-4}$ for the coarse and fine meshes, respectively.

Four simulations are performed in total with the only difference between them being the mesh. All meshes are unstructured, however two of them resolve the boundaries between the four regions and two of them don’t. For each of the two cases (resolving and non-resolving), a coarse and fine mesh simulation is performed.

Fig. 9 shows the gas phase saturation maps at time $t = 0.1$ along with the meshes used for all four simulations. Coarse meshes are located on the top, while fine meshes are located on the bottom. Non-resolving meshes are on the left, while region resolving meshes are located on the right. All four simulations are in good agreement and gas phase saturations follow similar patterns. Note that the differences between the region boundary resolving and non-resolving meshes are negligible.

Fig. 10 shows four gas phase saturation profiles at time $t = 0.1$ for all four simulations.

Now, we repeat the experiments using the P2DG-P2DG element pair. Figure 11 shows the gas phase saturation maps at time $t = 0.1$ along with the meshes used for all four simulations. Coarse meshes are located on the top, while fine meshes are located on the bottom. Non-resolving meshes are on the left, while region resolving meshes are located on the right. Comparing with the experiments using the overlapping mixed finite element method and the P1DG-P2 element pair, a better agreement between the results yielded from the coarse and fine mesh simulations is obtained.

4. An embedded-region modified Buckley-Leverett test case

Here a two-region permeability medium is solved. The low-permeability region with dimensions 0.5×0.5 is embedded in a high-permeability region with dimensions 1×1 . The permeabilities of the low-permeable region and high-permeable region are 10^{-4} and 1 respectively. The permeabilities of the porous medium and the unstructured mesh used are depicted in Figure 12. The porosity is uniform and equal to 0.5.

The initial, boundary conditions and physical properties used in Section 3 are considered for this problem.

Two different experiments are performed. One using the overlapping mixed finite element method and the P1DG-P1 element pair, and another using the P1DG-P1DG element pair. The time steps used are $5 \cdot 10^{-3}$ and 10^{-4} respectively.

Figure 13 and Figure 14 show the saturation profile at $t = 0.15$ and $t = 0.5$ respectively for the experiments using P1DG-P1 elements, left pictures, and P1DG-P1DG elements, right pictures. Both simulations yield a similar result. However, the experiments using P1DG-P1 elements show a dispersion of phase 1 into the low-permeability region whereas the saturation profile in the experiments using P1DG-P1DG elements present a defined frontier between the low-permeability region and the high-permeability area.

5. A wedge-shaped modified Buckley-Leverett test case

In this numerical experiment a wedge-shaped high-permeability (100) region embedded in a rectangular low-permeability (1) domain is considered, the permeability regions are depicted along with the unstructured mesh in Figure 15 . The non-dimensional rectangular domain is 1.0×0.1 and the wedge is defined by a height of 0.025 and a slope of $1/30$. The porosity is uniform and equal to 0.5.

Initially the porous media is filled by phase 2. In the simulation, phase 1 is injected from the left boundary with a constant pressure of 1 and a saturation of $S_g = 0.5$. On the outflow boundary the pressure level is set to zero. Free-slip boundary conditions are applied on the sides of the domain for the two velocity fields. All boundary conditions are applied weakly. The Corey model defined as: $k_g = S_g^{-2}$ is used to calculate the relative permeability.

Two different experiments are performed. One using the overlapping mixed finite element method and the P1DG-P1 element pair, and another using the

P1DG-P1DG element pair. The time steps used are 10^{-3} and 10^{-5} respectively.

Figure 16 and Figure 17 shows phase 1 saturation maps at time $t = 0.08$ and $t = 0.012$ respectively along with the meshes used for both simulations. In the experiments using P1DG-P1 elements we can see a dispersion of phase 1 in the vicinity of the wedge due to the continuous finite elements used for the saturation. On the other hand, the experiments using P1DG-P1DG elements shows a well-defined frontier of phase 1 within the wedge. It can be observed, that for this experiment the result obtained by both type of elements differ substantially.

6. Conclusions

Acknowledgements

This work was supported by the...

References

- Gomes, J., Pavlidis, D., Percival, J., Mostaghimi, P., Salinas, P., Xie, Z., Pain, C., Jackson, M., ELSheikh, A., Muggaridge, A., 2013. The overlapping control volume finite element method for multi-fluids porous media flow modelling. part i: Formulation. Computer Methods in Applied Mechanics and EngineeringSubmitted.

List of Figures

1	The continuous upwind method applied to the BL test case 1 for different mesh resolutions.	10
2	Saturation profiles for a number of element pairs and numerical resolutions in one and two dimensions. Top left: One dimension P0DG-P1, Top right: One dimension P1DG-P2. Bottom left: One dimension P2DG-P3. Bottom right: Two dimension P1DG-P2. The geometry symmetry line is used to extract data for the two-dimensional simulation.	11
3	L1 and L2 error convergence rates for a number of element pairs in one and two dimensions. Left: L1 error. Right: L2 error.	11
4	Gas phase saturation surface maps for a two- (left) and a three- (right) dimensional simulation of the Buckley-Leverett test case at time $t = 0.5$	12
5	Numerical experiments.	12
6	Saturation profiles for a number of element pairs and numerical resolutions in one and two dimensions. Top left: One dimension P0DG-P1, Top right: One dimension P1DG-P2. Bottom left: One dimension P2DG-P3. Bottom right: Two dimension P1DG-P2. The geometry symmetry line is used to extract data for the two-dimensional simulation.	13
7	L1 and L2 error convergence rates for a number of element pairs in one and two dimensions. Left: L1 error. Right: L2 error.	13
8	Four-region modified Buckley-Levrett test case schematic, including boundary conditions. The darker regions (R1 and R4) have high permeability.	14
9	Four-region modified Buckley-Levrett test case gas phase saturation maps at time $t = 0.1$. The meshes used for these simulations are also shown. Top left: coarse mesh. Top right: coarse, boundary resolving mesh. Bottom left: fine mesh. Bottom right: fine, boundary resolving mesh.	14

10	Four-region modified Buckley-Levrett test case gas phase saturation profiles at time $t = 0.1$. Top left: profiles at the diagonal starting at the bottom left corner of the domain. Top right: profiles at the diagonal starting at the top left corner of the domain. Bottom left: profiles at $x = 0.4$. Bottom right: profiles at $y = 0.4$	15
11	Four-region modified Buckley-Levrett test case gas phase saturation maps at time $t = 0.1$. The meshes used for these simulations are also shown. Top left: coarse mesh. Top right: coarse, boundary resolving mesh. Bottom left: fine mesh. Bottom right: (THIS PICTURE IS TEMPORAL, IT IS AT $t = 0.05$)fine, boundary resolving mesh.	16
12	The porous media consists of a low-permeability area embedded in a high-permeability region.	16
13	Gas phase saturation profile at time $t = 0.15$. The meshes used for these simulations are also shown. Left: Result using P1DG-P1 elements. Right: Result using P1DG-P1DG elements.	17
14	Gas phase saturation profile at time $t = 0.5$. The meshes used for these simulations are also shown. Left: Result using P1DG-P1 elements. Right: Result using P1DG-P1DG elements.	17
15	The porous media consists of a high-permeability wedge-shaped area in a low-permeability rectangle.	18
16	Gas phase saturation profile at time $t = 0.08$. The meshes used for these simulations are also shown. Up: Result using P1DG-P1 elements. Down: Result using P1DG-P1DG elements.	18
17	Gas phase saturation profile at time $t = 0.12$. The meshes used for these simulations are also shown. Up: Result using P1DG-P1 elements. Down: Result using P1DG-P1DG elements.	18

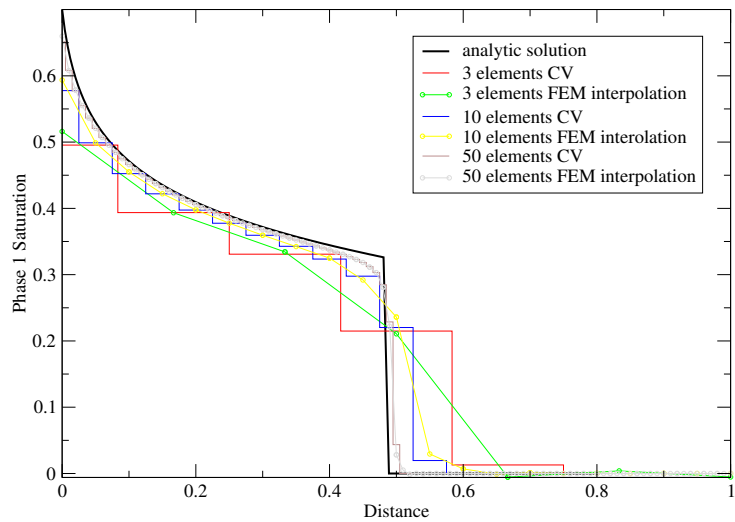


Figure 1: The continuous upwind method applied to the BL test case 1 for different mesh resolutions.

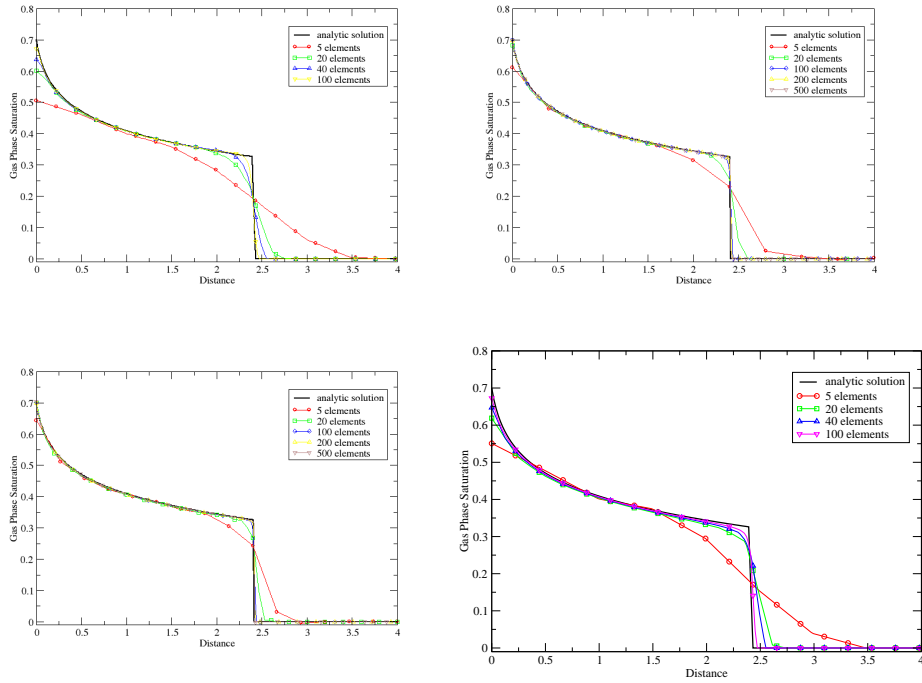


Figure 2: Saturation profiles for a number of element pairs and numerical resolutions in one and two dimensions. Top left: One dimension P0DG-P1, Top right: One dimension P1DG-P2. Bottom left: One dimension P2DG-P3. Bottom right: Two dimension P1DG-P2. The geometry symmetry line is used to extract data for the two-dimensional simulation.

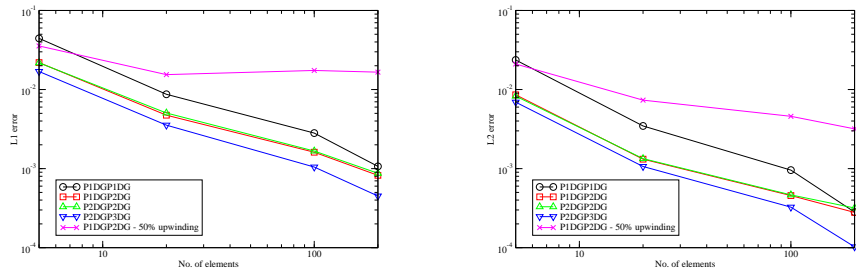


Figure 3: L1 and L2 error convergence rates for a number of element pairs in one and two dimensions. Left: L1 error. Right: L2 error.

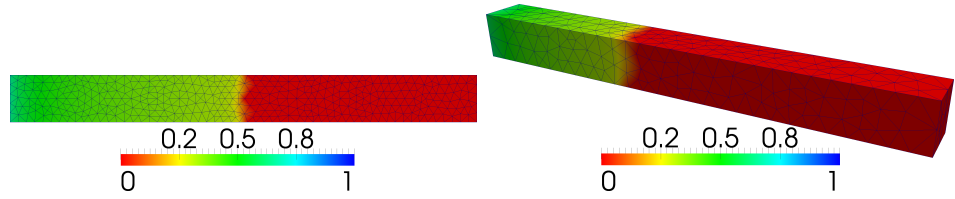


Figure 4: Gas phase saturation surface maps for a two- (left) and a three- (right) dimensional simulation of the Buckley-Leverett test case at time $t = 0.5$.

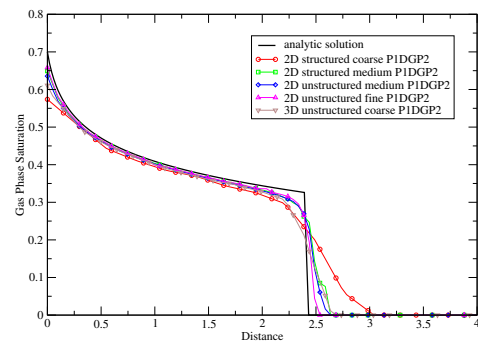


Figure 5: Numerical experiments.

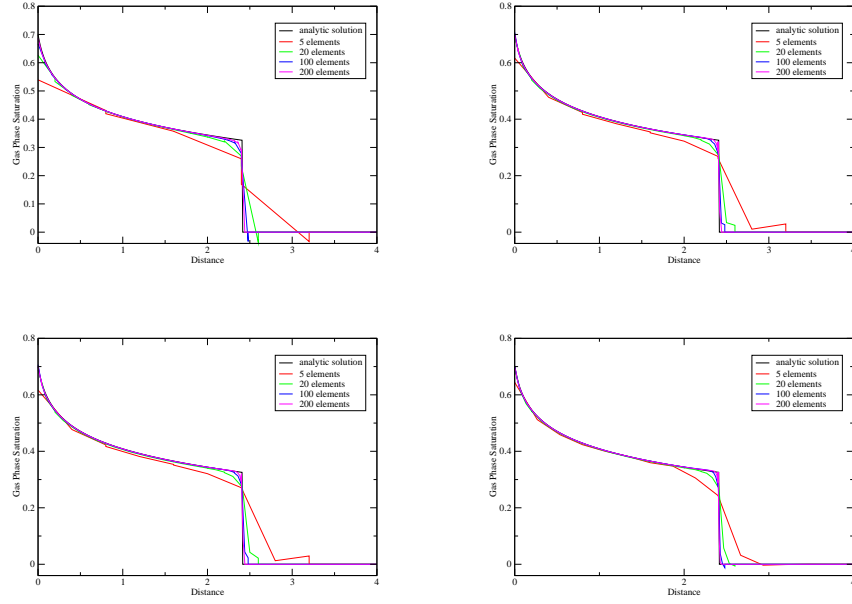


Figure 6: Saturation profiles for a number of element pairs and numerical resolutions in one and two dimensions. Top left: One dimension P0DG-P1, Top right: One dimension P1DG-P2. Bottom left: One dimension P2DG-P3. Bottom right: Two dimension P1DG-P2. The geometry symmetry line is used to extract data for the two-dimensional simulation.

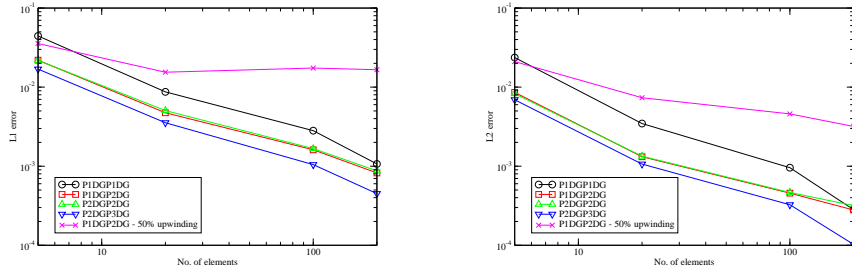


Figure 7: L1 and L2 error convergence rates for a number of element pairs in one and two dimensions. Left: L1 error. Right: L2 error.

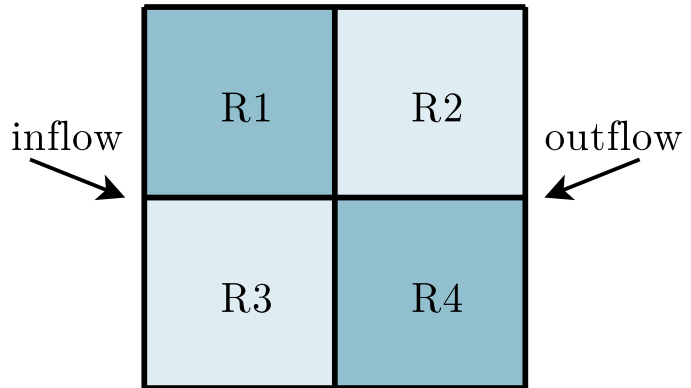


Figure 8: Four-region modified Buckley-Levrett test case schematic, including boundary conditions. The darker regions (R1 and R4) have high permeability.

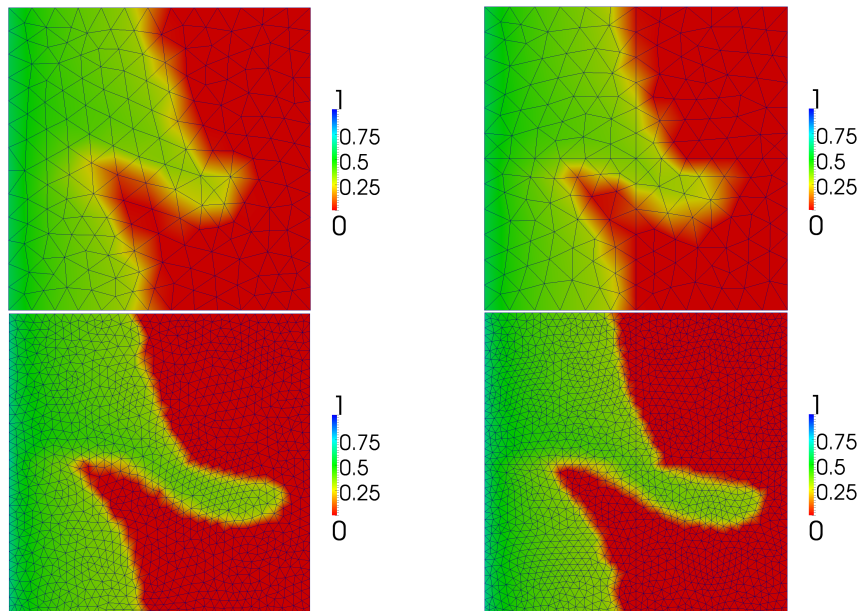


Figure 9: Four-region modified Buckley-Levrett test case gas phase saturation maps at time $t = 0.1$. The meshes used for these simulations are also shown. Top left: coarse mesh. Top right: coarse, boundary resolving mesh. Bottom left: fine mesh. Bottom right: fine, boundary resolving mesh.

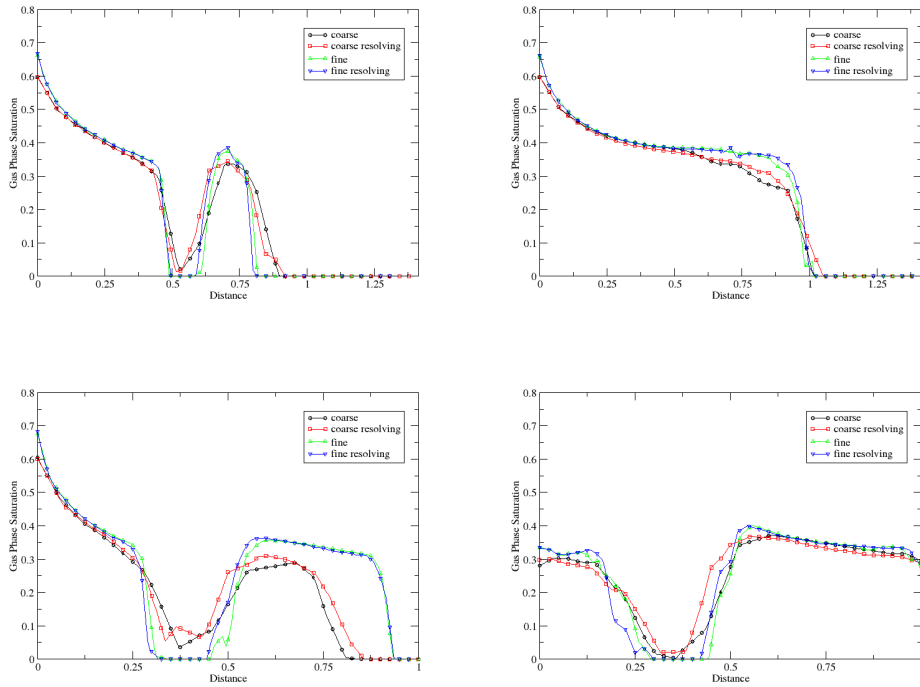


Figure 10: Four-region modified Buckley-Levrett test case gas phase saturation profiles at time $t = 0.1$. Top left: profiles at the diagonal starting at the bottom left corner of the domain. Top right: profiles at the diagonal starting at the top left corner of the domain. Bottom left: profiles at $x = 0.4$. Bottom right: profiles at $y = 0.4$.

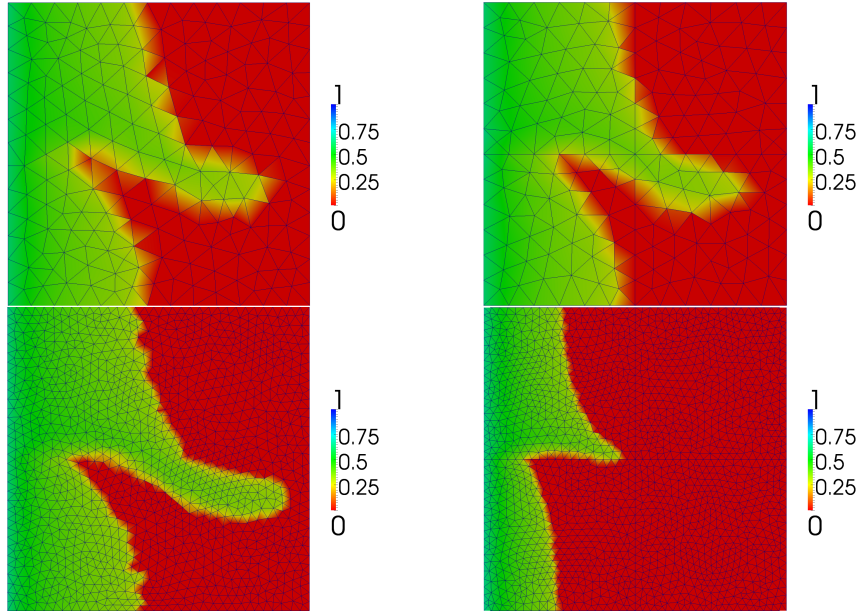


Figure 11: Four-region modified Buckley-Levrett test case gas phase saturation maps at time $t = 0.1$. The meshes used for these simulations are also shown. Top left: coarse mesh. Top right: coarse, boundary resolving mesh. Bottom left: fine mesh. Bottom right: (THIS PICTURE IS TEMPORAL, IT IS AT $t = 0.05$) fine, boundary resolving mesh.

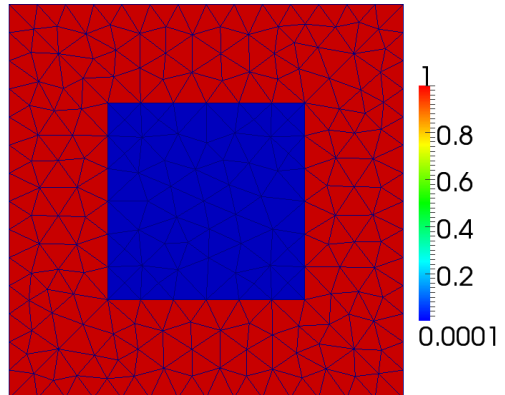


Figure 12: The porous media consists of a low-permeability area embedded in a high-permeability region.

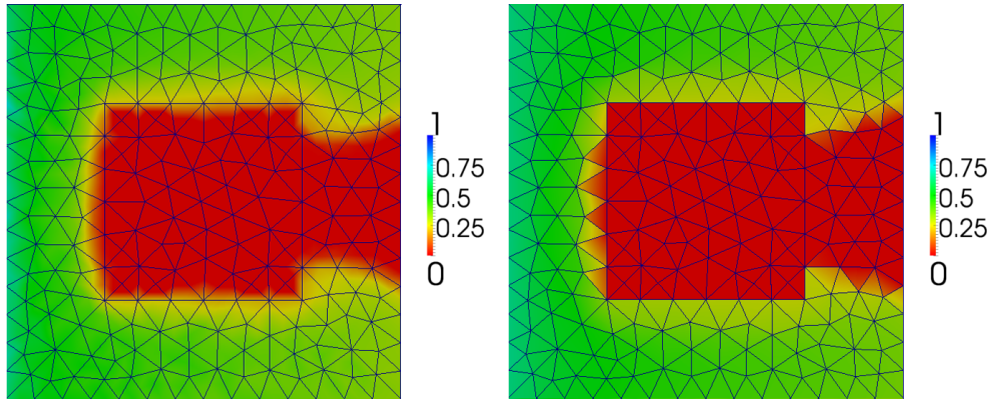


Figure 13: Gas phase saturation profile at time $t = 0.15$. The meshes used for these simulations are also shown. Left: Result using P1DG-P1 elements. Right: Result using P1DG-P1DG elements.

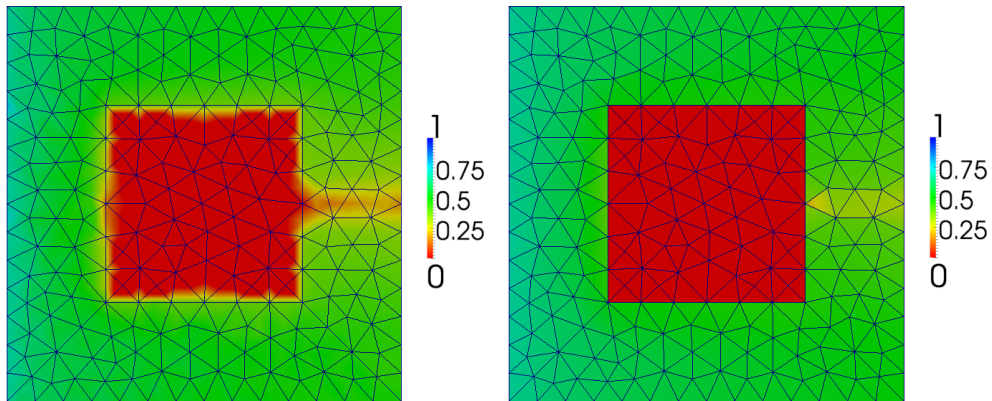


Figure 14: Gas phase saturation profile at time $t = 0.5$. The meshes used for these simulations are also shown. Left: Result using P1DG-P1 elements. Right: Result using P1DG-P1DG elements.



Figure 15: The porous media consists of a high-permeability wedge-shaped area in a low-permeability rectangle.

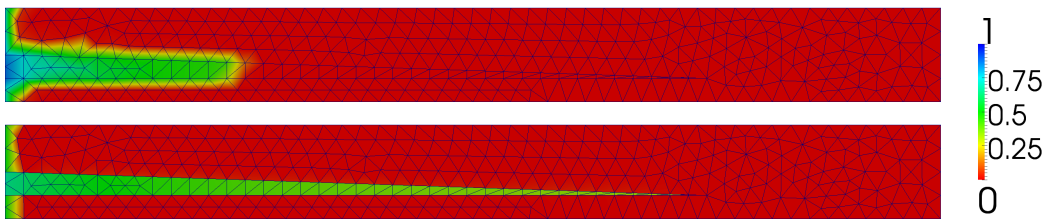


Figure 16: Gas phase saturation profile at time $t = 0.08$. The meshes used for these simulations are also shown. Up: Result using P1DG-P1 elements. Down: Result using P1DG-P1DG elements.

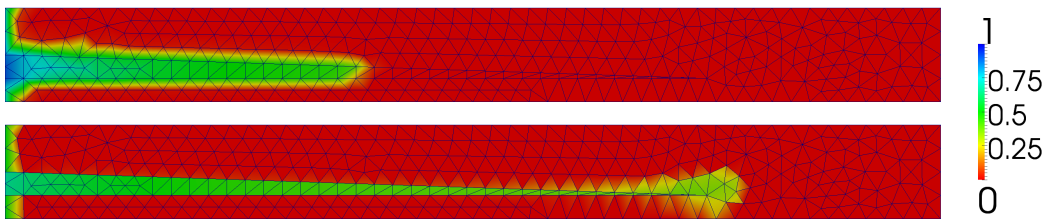


Figure 17: Gas phase saturation profile at time $t = 0.12$. The meshes used for these simulations are also shown. Up: Result using P1DG-P1 elements. Down: Result using P1DG-P1DG elements.